Bull. Disas. Prev. Res. Inst., Kyoto Univ., Vol. 26, Part 1, No. 234, March, 1976

Some Problems of Seismic Data Processing
Part 3. Particle Motion Analysis of Local Earthquake Waves and the Underground Structure beneath Recording Sites

By Tamotsu FURUZAWA

(Manuscript received March, 1, 1976)

Abstract

The ground particle motions of seismic waves obtained from the short-period observational system and the system of automated analysis, which has been successfully employed at the Amagase station as described in previous papers, are analyzed to examine the accuracy of informations and the relation to the local crustal structures. The angles of incidence of P and SV waves and the direction of particle motion of P wave in the horizontal plane are discussed on the basis of data from both quarry blasts and local earthquakes with known epicenters.

1. Introduction

The wave-analysis with high accuracies based on digital techniques has been applied so far mainly to teleseismic or long-period waves but little to local earthquake waves. This may be ascribed to the fact that an application of digitizing techniques to the seismograms with high frequency and short duration has not been practically so easy. Since these difficulties are expected to be overcome to a considerable extent by using the new observational system described in Part 1[1a], it may be useful to apply the digital analysis to local earthquake waves to get information on the ground particle motions and their relation to local underground structures.

The system for automated analysis of local earthquakes recorded at one observational site with a three component set of short-period seismometers was described in Part 2[1b]. The main objectives were to find a reliable method of automated identification of *P* initial phase and *S* wave motions as the first stage of seismological data flow described by Keilis-Borok[2], and to carry out the frequency analysis of *P* and *S* waves. The automated analysis described in Part 2 has been used only to the seismograms recorded at one site. However, any array system based on the assumption of uniform structure at each site is scarcely real in geologically complicated regions. And the method of correlogram processing based on seismic array is not always appropriate to the phase identification of local earthquake waves, even if the data were obtained from several observational sites. In particular, for the identification of *S* phase, the use of three-component data obtained at each site will be the only way we can apply. Consequently, the analysis system as described in Part 2 gives much contribution to the above purposes, and has been already practically operated at the Amagase station.

In this paper, the results obtained from the records at the other sites in the vicinity of Amagase are incorporated and described in some detail. As the result of this analytical procedure, various information on particle motins of P and S waves in both the horizontal and vertical planes has been obtained. A detailed analysis of particle motions is very important not only for the identification of various phases, particularly of S phase, but also for the investigation of the source or the propagation path. The relations of the observed particle motions to the local structure near recording sites are described here using data from both quarry blasts and local shocks with known epicenters.

2. Observation and Data Preparation

Short-period seismograms recorded at the Amagase station (abbreviated by AMA) were primarily used for analysis of particle motions. To examine the availability of the analytical system described in Part 2, the seismograms recorded at Ohbaku (OHB), Sumiyama (SUM) and the Uji campus (CMP) of Kyoto University were also used in comparison with those of Amagase. The locations of observational sites are shown in Fig. 1. At the Amagase site, seismometers have been set up on rock at 500 m from the entrance of an observational gallery and at a depth of 140 m. The OHB and SUM sites are situated on exposed rock on the west and east sides

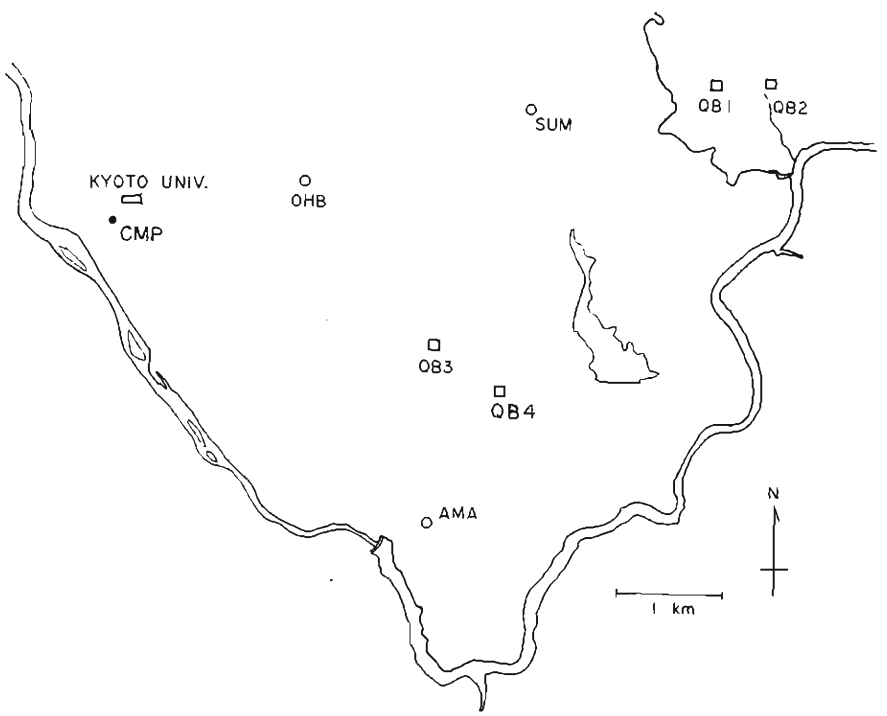

Fig. 1. Location of observational points (circles) and quarry sites (squares).

of Mt. Gounho, respectively, and CMP is on soft sediment. Seismograms at AMA were obtained from the routine observations using the new system described in Part 1, which have been continuously operated since 1974, and also from the temporary observations with magnetic tape recorder, which were made during one month in every summer from 1969 to 1972. Observations at OHB and CMP have been carried out by the routine system with time-delay operator consisting of a magnetic drum.[3] At the SUM site, temporary observations were carried out during 6 weeks from November to December, 1974. The instruments used at each site are 3-component sets of short-period seismometers with a natural period of 1.0 sec, damping factor of h=0.64 and sensitivity of 3.0 V/kine. The amplifiers were operated with gains of 650 in routine and 1000 in temporary observations at AMA, 500 at OHB and SUM, and 50 at CMP, respectively.

In Fig. 1, QB-1, 2, 3 and 4 show the shot points at quarry sites. Observations were also carried out immediately near quarry sites. This enables us to obtain both the accurate shot time and the waveform records at the source.

The seismograms from a number of local earthquakes recorded at the four sites were digitized with sampling interval of 0.01 sec through the 25 Hz low-pass filter. For records from quarry blasts, a finer sampling interval of 0.003 sec was used with cut-off frequency of 31.5 Hz.

3. System of Analysis

The automated system of analysis described in Part 2 was used for the particle motion analysis. For this purpose, the validity of this system is extensively tested in this section, using the data obtained at OHB, SUM and CMP, in addition to the data at AMA. The present system can be operated for the discrimination of *P* and *S* waves under the following assumptions:

(1) Both the spectral shape and amplitude level between noise and *P* wave portions have some differences.
(2) The directional distribution of particle motion of noise is random in both time and frequency.
(3) The noise spectra are nearly stationary in time.
(4) The particle motion of initial *P* waves has a good rectilinearity.
(5) There are no remarkable converted phases between direct *P* and *S* waves.
(6) The spectra of *S* waves are not same as those of *P* waves.

The noise spectra of vertical component seismograms recorded at AMA, which have been evaluated through time window of 0.64 sec at an interval of the order of one year, are shown in Fig. 2. Although fine peaks and troughs of the spectra are different from each other, it is noticed that the general spectral shape over low to high frequencies does not significantly change with time, and hence may be regarded as practically stationary. Minor undulations in the noise spectra would not give serious effects to identify the initial *P* waves, because only differences in the general shape between *P* and noise spectra are important for the present purpose.

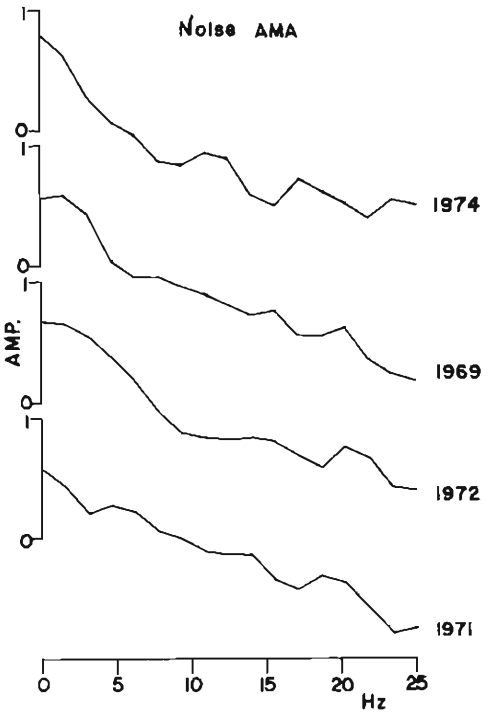

Fig. 2. Comparison of noise spectra of vertical components at AMA with respect to time.

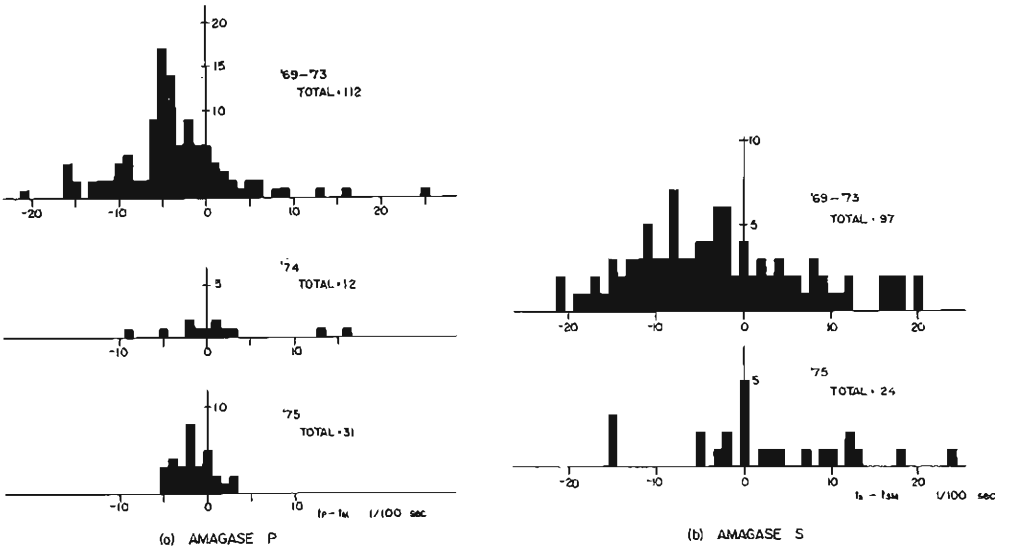

Fig. 3. Histograms of the differences between onsets determined from automated method, t_P, and those read visually, t_M, every 0.01 sec.
(a) For *P* waves, (b) For *S* waves.

Fig. 3(a) shows the histograms of the differences between the P onset time determined from automated method, t_P, and those read visually, t_M. A rather broad distribution of the differences for the 1974 data is attributable to the effect of noise due to troubles with the time-delay equipment used. For the 1975 data, the situation has been quite improved, since the effect of side lobe of the band-pass filter was introduced into the conditions for discrimination. And so it resulted that the onset time of P first arrival for all events (total 31) could be determined within ± 0.05 sec. Fig. 3(b) shows similar histograms for S waves. The extent of the distribution is broader than that for P waves, but it indicates almost similar features in time. It may be considered that these results reflect both the stationary characteristics of noise at AMA and the reliability of the discriminative conditions.

In Fig. 4, the spectra of P waves from a local shock and that of noise obtained at three sites of AMA, OHB and SUM are compared. The P wave-spectra at the latter two sites on the surface fall off rapidly with increase of frequency, whereas those at

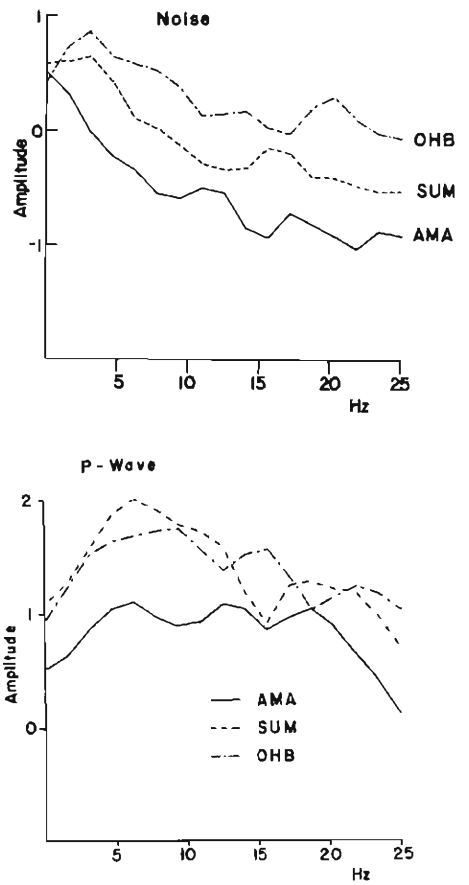

Fig. 4. Spectra of P and noise parts of the same event recorded at AMA, SUM and OHB.

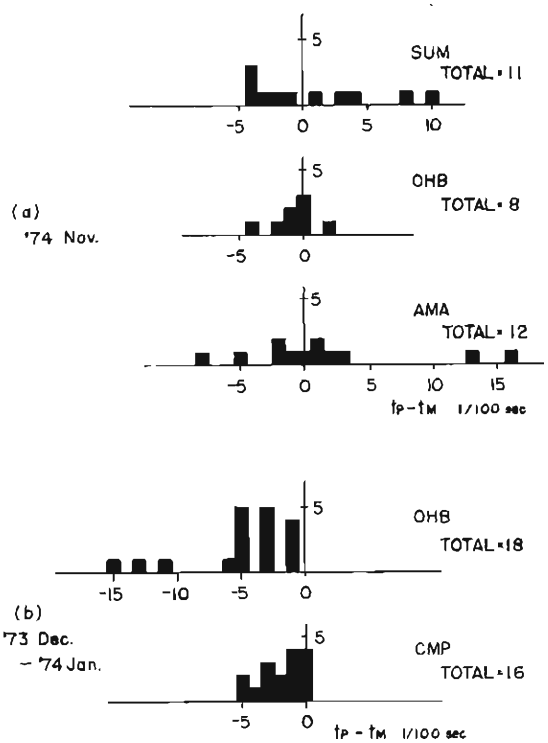

Fig. 5. Histograms of the differences of P onset times, $t_P - t_M$, compared for results applied to the different sites.
(a) Comparison of the three sites, AMA, SUM and OHB.
(b) Comparison of the two sites, OHB and CMP.

AMA are almost flat over the broad frequency band. Also, the amplitude level in the low frequency range up to about 12 Hz is significantly higher than at AMA. Fig. 5(a) shows the results for 12 events recorded at three sites, which have been obtained on the basis of the same discriminative conditions. As seen from Fig. 5(a), the results obtained at three sites are similar with each other, although the spectral characteristics of both P waves and noise are not always similar. The results obtained at OHB and CMP are also shown in Fig. 5(b), as examples for unfavourable conditions. In the case of CMP, the discriminative condition has been somewhat modified to suite the high noise level. It is to be noted that even in this case the P onset time could be determined within ± 0.05 sec.

Fig. 6 shows three component waveforms of P intial portions recorded at AMA, OHB and SUM, which have been obtained through a D–A converter. As the amplitude has been normalized independently at each site when displayed on an X–Y plotter, the amplitude levels can not be directly compared. "P" shows the P onset determined from the automated method. Two arrows indicate the windows over which P-spectra have been computed. Because the particle motion of P waves has a rather poor rectilinearity, there are some apparent transverse com-

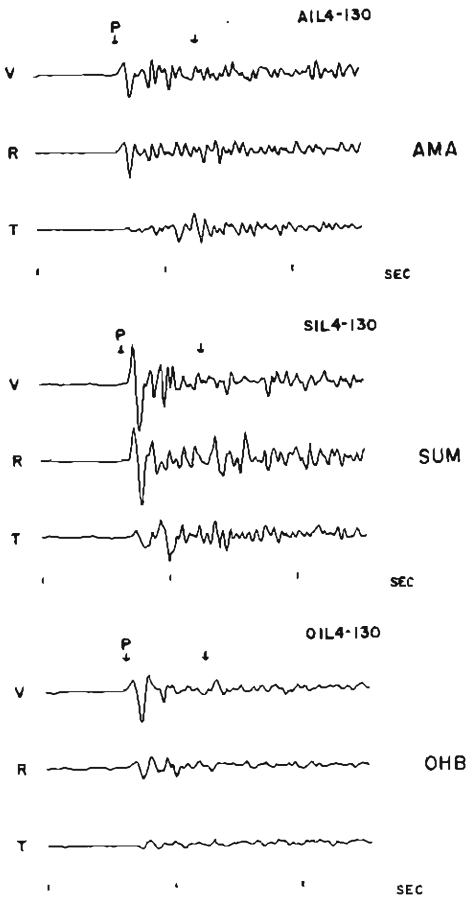

Fig. 6. D–A converted waveforms around *P* initial part at the three sites, AMA, OHB and SUM. "*P*" shows the *P* onset determined from automated method. Interval between two arrows indicates the window for *P*-spectra.

ponents just after *P* onset at SUM and OHB. Thus, for these two sites, the present examination of the characteristics of particle motion should be considered insufficient to analyze *S* waves.

This automated analysis system gives the onset times, the direction and rectilinearity of particle motions and the spectra of *P*, *SV* and *SH* waves as outputs on a line-printer, and also the original and band-pass filtered waveforms of both *P* and *S* waves, the particle motion diagrams and spectra are displayed on an X–Y plotter. In the next section, the particle motion diagrams obtained by this procedure will be used for the analysis.

4. Results and Discussions of Particle Motion Analysis

4-1. P and S velocities of the surface layer

Travel time data from quarry blasts marked as QB–1, 2 and 3 in Fig. 1 are illustrated in Fig. 7, which were obtained under the assumption of an uniform structure over the path from the quarry to recording sites. Open and closed circles correspond to the data obtained at AMA and at the other sites, respectively. The P velocity is found to be 4.66 km/sec from the least-squares fit to these data. The surface layer having this velocity probably extends laterally over 5 km near AMA, which is underlain by the second layer with the velocity of 5.5 km/sec estimated by the Research Group for Explosion Seismology[4]. The lack of head waves from an underlying layer at an epicentral distance within 5 km suggests that the thickness of this layer extends no less than 700 m beneath the surface.

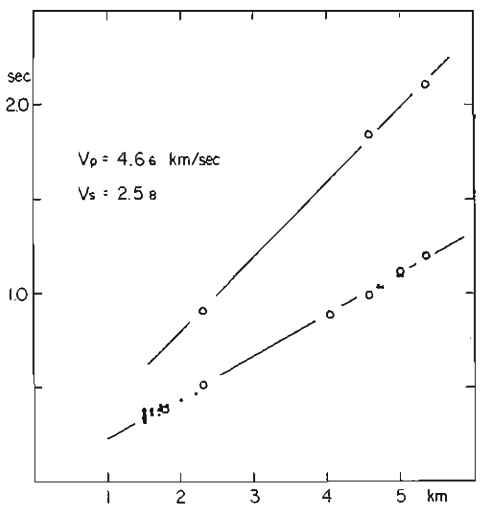

Fig. 7. Travel time of P and S waves from quarry blasts.

Fig. 8 illustrates both the waveforms recorded at AMA and the particle motion diagrams in the vertical plane, in the case of QB–1. SV arrival can be identified from the change in the direction of particle motions at interval No. 3 in the frequency bands of 10–15 and 15–20 Hz. The dashed arrows on the V and R traces represent the initial onset of SV motion. At almost the same time as the SV onset, the arrival of a distinct phase is also found on the transverse component. The low frequency phases following SV waves have retrograde particle motions, and hence they may be surface waves. The travel times of SV waves identified in this way are plotted against distances in Fig. 7, and the S wave velocity is estimated as 2.58 km/sec.

4-2. Angles of incidence of P waves

The angles of incidence of P motion from quarry blasts are listed in Table 1. i_{obs}

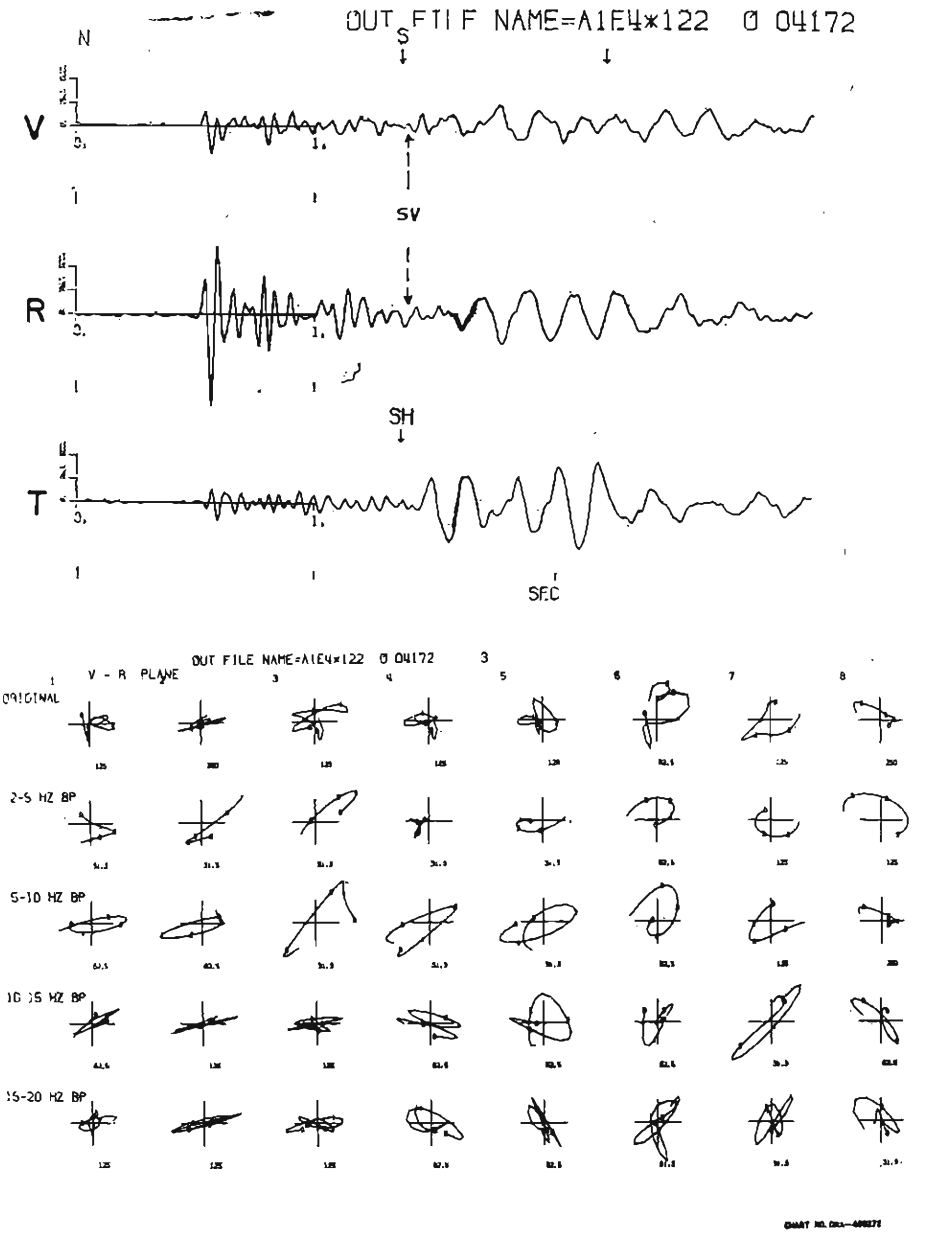

Fig. 8. Three components (V, R, T) seismograms of quarry blast (QB–1) observed at AMA, and particle motion diagrams of original and band-pass filtered seismograms in the vertical plane.

represents the apparent angle of incidence determined from the particle motion diagrams in the vertical plane using the first one-cycle in the frequency bands of 10–15 and 15–20 Hz (interval No. 2 in Fig. 8). More than two measured values of

Table 1. Angles of Incidence of *P* Initial Motion from Quarry Blasts

Sites	Distance km	i_{obs}	i_{model}
QB 4	1.45	80°, 82°	80.4°
QB 3	1.75	80°	78.7°
QB 1	4.98	71°, 72°, 73°, 74°	74°

i_{obs} from the same quarry site agree with each other within 3°. It is also noticed that i_{obs} decreases with increasing epicentral distances. The differences between 80°–82° at distances of 1.4–1.8 km and 71°–74° at distance of 5 km exceed the measurement error of 3° above described, suggesting the increased velocity with depth. If the velocity increases linearly with depth, as expressed by $V=V_0+kZ$, then the travel-time, T, the angle of incidence, i, the epicentral distance, Δ, and the velocity at the deepest point of the ray, V_m, are related by the following relations,

$$T=2/k \sin^{-1}\left(\frac{k\Delta}{2V_0}\right) \tag{1}$$

$$\sin i=V/V_m \tag{2}$$

$$V_m=V_0\sqrt{1+\left(\frac{k\Delta}{2V_0}\right)^2}\,. \tag{3}$$

For $\Delta=4.98$ km, $T=1.09$ sec, and $i=74°$,

$$V=4.52+0.5\,Z. \tag{4}$$

The angles of incidence calculated from this velocity structure are also listed in Table 1 as i_{model}. It is found that i_{obs} and i_{model} are in good agreement within about 2°. On the other hand, the differences of travel times between this velocity structure and an uniform velocity of 4.66 km/sec become 8 msec at $\Delta=1.5$ km and 0 at $\Delta=5$ km. It is, therefore, difficult to discuss discrepancies less than 10 msec on the basis of such an observational travel-time curve as shown in Fig. 7. This suggests that the angles of incidence may provide better resolution on fine velocity structures.

4-3. The direction of particle motion of P waves in the horizontal plane

The particle motions of *P* waves in the horizontal plane show the best rectilinearity and directionality in the frequency band of 10–15 Hz, as illustrated in Fig. 9, while for frequency bands lower than 10 Hz, the rectilinearity tends to become worse. In higher frequency bands, on the other hand, the direction of motion tends to deflect to the north-south. This tendency probably reflects the local effect due to fine structural irregularities. Thus, the direction of particle motion in the frequency band of 10–15 Hz may be used with highest accuracy to infer the direction of wave approach. For local shocks with *S*–*P* times below 5 sec, the deviations of the inferred direction relative to the corresponding epicentral direction are plotted against azimuth in Fig. 10, where the data of epicenters were obtained from the routine observations for microearthquakes. The positive values in Fig. 10 indicate

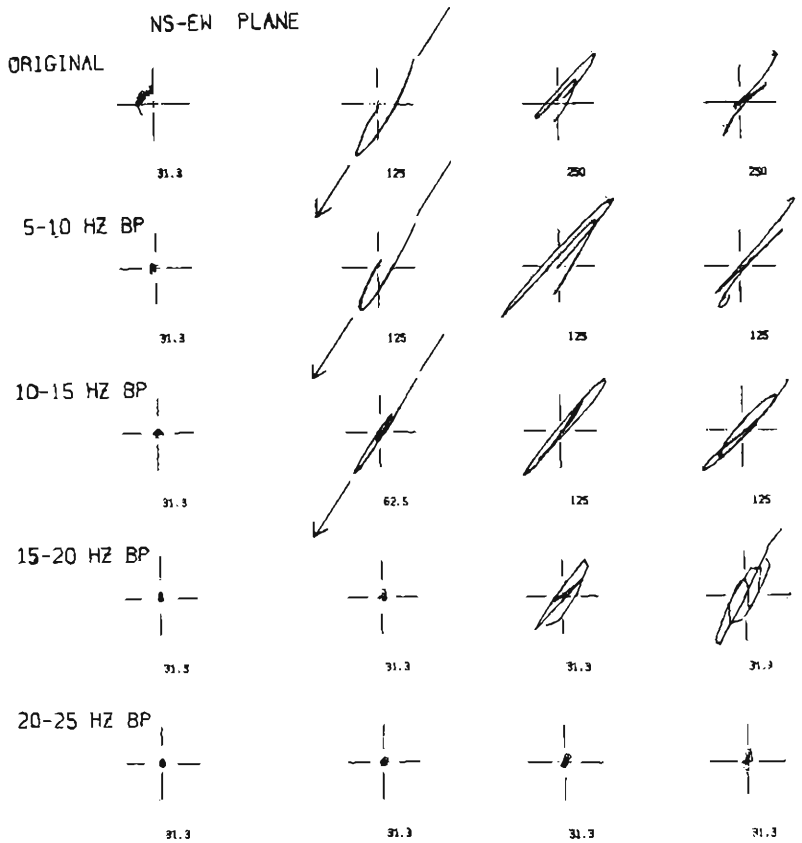

Fig. 9. An example of particle motion diagrams of *P* initial motion in the horizontal plane obtained from original and band-pass filtered seismograms. Arrows indicate the direction of epicenter.

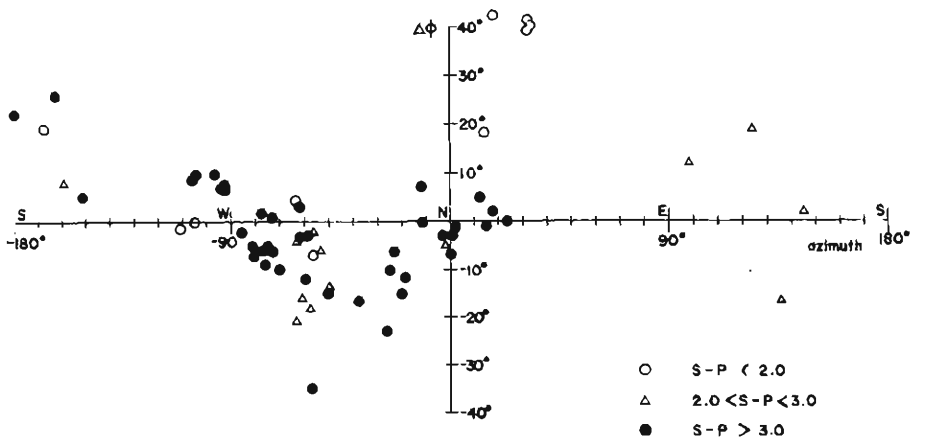

Fig. 10. Deviation of the arrival direction of *P* wave from the direction of source in the 10–15 Hz band, as a function of azimuth.

the clockwise deviation to the direction of epicenter and the negative values indicate the counter-clockwise deviation.

For the events with S–P times above 3 sec, the deviations seem to be systematic. That is, the arrival direction of P wave deflects westwards with the maximum deviation in the northwest direction, although there are practically no deviation in the due north and west, and eastwards deviations around the south. For the events with S–P times below 3 sec, it may also be said with less reliability because of a small number of data, that the deviations are not inconsistent with those for the former class of events. For the quarry blasts, on the other hand, the direction of P arrival and the azimuth to the source are in agreement with an accuracy within 1 or 2 degrees. This means that the above deviations cannot be attributed to noise, errors in system calibration, or errors in seismometer placement.

For events in the northwest to southwest regions, for which the determination of epicenters may be reliable in view of appropriate coverage of observational points, the deviations could be interpreted to come from a dipping layer toward the east beneath Amagase. The absolute value of deviation at specific azimuth should be dependent on the angle of incidence. For the events studied here, the angles of incidence of P waves determined from particle motions range from 40° to 60°. Assuming the velocities of 4.6 km/sec for the surface layer and 5.5 km/sec for the second layer, respectively, the dip of interface between the two layers would have to be greater than 40°, referring to the results of Niazi (1966)[5] to explain the deviation of about 15° in the northwest direction. Furthermore, if the deviations in the NW to N directions are similarly explained by the effects of a dipping layer, a steep dip toward the north would be required. Thus, it appears that there is a lateral transition into two structures which has different dip directions in the northwest of AMA. It is possible, however, that more complicated geological structures than was assumed here could cause these azimuth deviations.

4-4. Angles of incidence of SV waves

Under the assumption of plane harmonic waves, the surface particle motion of S waves is linear only for angles of incidence less than $\sin^{-1}(V_S/V_P)$[6]. This critical angle at AMA is estimated to be about 33° from the P and S velocities near the surface. The particle motion diagram of P and S portions for an event with S–P time of 2.20 sec is shown in Fig. 11. The apparent angle of incidence of P initial motion from this event is found to be 44°, and hence the true angle of incidence becomes 46°. For a homogeneous medium, the angle of incidence of S wave motions should be approximately equal to that of P. Therefore, the surface particle motion of S waves in the present case should be nonlinear due to greater angles of incidence than the critical. Nevertheless, the particle motion of SV waves initiating from the fifth interval in Fig. 11 exhibits good linearity, and its apparent angle of incidence may be determined as about 27° from the diagram. This means that the estimated angle of incidence of S waves significantly differ from that of P waves. This low apparent angle of incidence and linearity of the SV motion are commonly observed

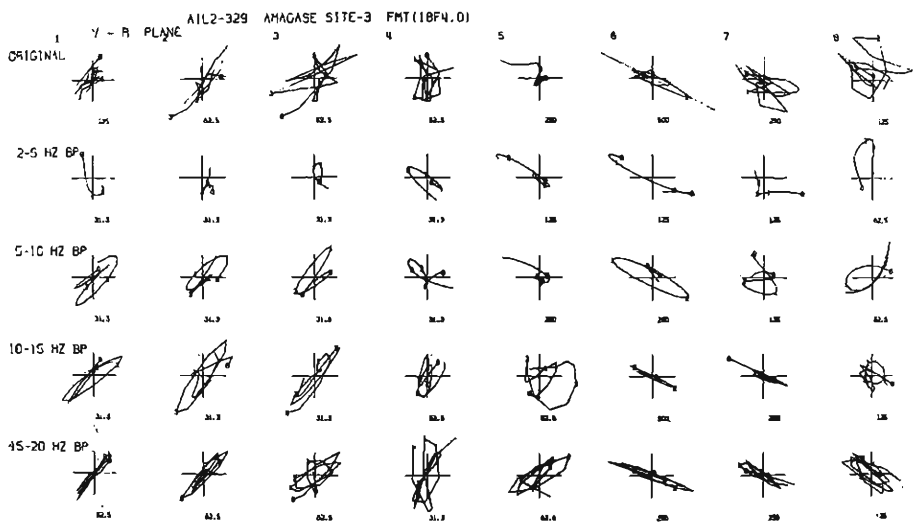

Fig. 11. Particle motion diagram of *P* and *S* portions of event with *S*–*P* times of 2.20 sec in the vertical plane.

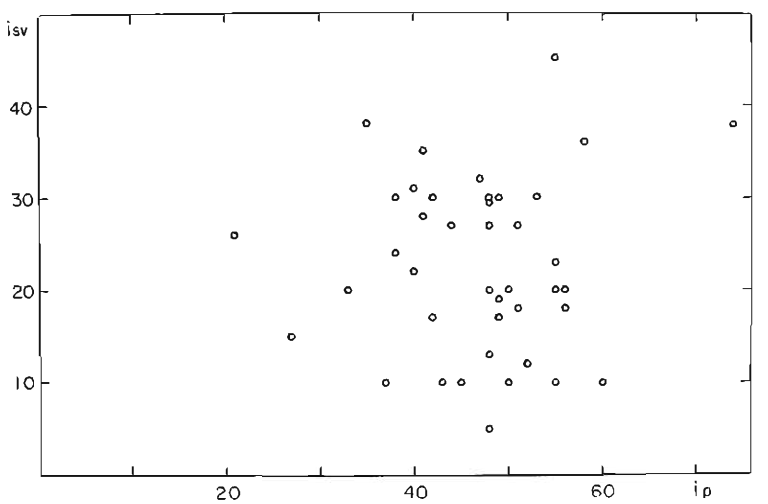

Fig. 12. Relations of apparent angles of incidence of *P* and *SV* waves determined from particle motion diagrams.

for the other events treated in the present study. The apparent angles of incidence of *P* and *SV* waves thus determined are plotted in Fig. 12. The linearity of the *SV* motion at distances up to 70 km was also described by Filson (1970)[7]. These results might suggest either that the plane wave theory cannot be aplied without any corrections for such near distances as several tens of kilometers, or that the crust has a strong *S*-velocity gradient. Moreover, it must be taken into consideration that the effect of free surface varies depending on frequency, since the AMA site is

located at some depth from the surface[8].

5. Conclusion

From the comparison of the results obtained at three observational sites, AMA, OHB and SUM, it may safely be concluded that the system of automated analysis for *P* waves described in Part 2 can well be widely used for ordinary seismograph stations. For *S* waves, however, the system may be applied only to the sites where the characteristics of *P*-wave particle motions are well known.

The present system gives the onset times, the azimuths of wave arrival, the angles of incidence and the Fourier spectra of *P*, *SV* and *SH* waves as outputs in a printed form, and also the particle motion diagrams in both the horizontal and vertical planes and the filtered waveforms in different frequency bands are plotted on an X–Y plotter. Since lengthy and tedious procedures in similar analysis made by a conventional way could be considerably lessened by the use of our analysis system, it may said that a significant enhancement of the efficiency in digital analysis has been attained.

In the present paper, an emphasis has been laid to examine the relation between the particle motions of body waves and local crustal structure near observational sites, using the reliable information obtained from the above analysis procedure. The angles of incidence of *P* initial motions from quarry blasts suggest a linearly increased velocity with depth in the surface layer. The deviations of the direction of *P* wave particle motions in the horizontal plane from the epicentral direction could be interpreted qualitatively by the effects of dipping layers beneath Amagase. To make quantitative discussions, however, more accurate data of epicenters are required. For the apparent low angles of incidence and linearity of *SV* motions at near distances obtained from the present study, further detailed discussions should be made in future, taking into account shear motions at the source and the effects of complicated structures on the polarization of *S* waves.

More complete interpretations for these results will be obtained from analysis of the data observed at two other sites, OHB and SUM, but it should be necessary to examine topographycal effects of the recording sites prior to the particle motion analysis.

Acknowledgements

The author wishes to express his sincere thanks to Dr. Tatsuhiko Wada of Kyoto University for much valuable advice and encouragement in carrying out this work, and also to Prof. Michio Takada for his encouragement. The author is indebted to Messrs. Junpei Akamatsu, Kojiro Irikura and Shuzo Takemoto, his colleagues, for their valuable discussions and co-operation in carrying out observations and in programming for the various computations, and to Mr. Akio Hirono for his helpful assistance to the observations. Special thanks are due to Prof. Takeshi Mikumo

for critically reading the manuscript, offering constructive criticism.

The data processing was run on a FACOM 230–25 at the Information Data Processing Center for Disaster Prevention Research of the Disaster Prevention Research Institute of Kyoto University.

References

1a) Furuzawa, T.: Some problems of seismic data processing, Part 1 Bull. Disast. Prev. Res. Inst. Kyoto Univ., Vol. 24, 1974, pp. 49–66.

1b) Furuzawa, T.: Some problems of seismic data processing, Part 2, Bull. Disast. Prev. Res. Inst., Kyoto Univ., Vol. 24, 1974, pp. 127–145.

2) Кейлис-Борок, В. И.: Сейсмология и логика, Вычислительная сейомология, Вып. 4, Наука, 1968, 317-350.

3) Irikura, K. and J. Akamatsu: Earthquake motions observed on rock and ground, Bull. Disast. Prev. Res. Inst., Kyoto Univ., Vol. 24, 1974, pp. 263–280.

4) Mikumo, T., M. Otsuka, T. Utsu, T. Terashima and A. Okada: Crustal structure in central Japan as derived from the Miboro explosion-seismic observations, Part 2, Bull. Earthq. Res. Inst., Tokyo Univ., Vol. 39, 1961, pp. 326–349.

5) Niazi, M.: Corrections to apparent azimuths and travel time gradients for a dipping Mohorovicic discontinuity, Bull. Seism. Soc. Am., Vol. 56, 1966, pp. 491–509.

6) Nuttli, O.: The effect of the earth's surface on the S-wave particle motion, Bull. Seism. Soc. Am., Vol. 51, 1961, pp. 237–246.

7) Filson, J.: S velocities at near distance in western central California, Bull. Seism. Soc. Am., Vol. 60, 1970, pp. 901–915.

8) Furuzawa, T., K. Irikura, S. Takemoto and J. Akamatsu: Spectra of body waves from local small earthquakes in the southern parts of Kyoto, Bull. Disast. Prev. Res. Inst., Kyoto Univ., Vol. 22, 1972, pp. 23–36.